ISIJ International, Vol. 60 (2020), No. 2, pp. 337–345

Passivation Mechanism of Galvanized Steel Rebar in Fresh Concrete

Mari MAEDA,[1)]* Xiuyang LI,[2)] Azusa OOI,[1)] Eiji TADA[1)] and Atsushi NISHIKATA[1)]

1) School of Materials and Chemical Technology, Tokyo Institute of Technology, 2-12-1 Ookayama, Meguro-ku, Tokyo, 1528550 Japan.
2) JGC Corporation, 2-3-1 Minatomirai, Nishi-ku, Yokohama, Kanagawa, 2206001 Japan.

(*Received on July 1, 2019; accepted on August 5, 2019*)

We studied the passivation behavior of hot-dip galvanized steel (HDG) rebar and ordinary steel (black) rebar in fresh concrete using electrochemical techniques. Although the passivation behavior was considerably different, both types of rebar were fully passivated. The black rebar was immediately passivated after exposure to fresh concrete; however, the HDG rebar was passivated after being kept active for tens of hours. The corrosion rates of both types of rebars after passivation seemed comparable. To further investigate the difference, we monitored the passivation processes by electrochemical impedance spectroscopy using carbon steel and zinc electrodes in fresh mortar and saturated $Ca(OH)_2$ solution, which simulated the water in the concrete pores; furthermore, we observed similar trends for fresh concrete. Initially, the Zn surface was partially covered with calcium hydroxy zincate (CHZ) whose coverage increased with exposure time. Finally, the surface was fully covered with a CHZ film after passivation.

KEY WORDS: galvanized steel rebar; zinc; passivation; concrete; calcium hydroxy zincate; electrochemical impedance spectroscopy.

1. Introduction

Steel bar-reinforced concrete has been extensively used in buildings and civil engineering structures, where the steel bar is passivated in sound concrete. However, the pH gradually decreases because of the penetration of CO_2 in air via the concrete, leading to the depassivation of the rebar surface. In the marine environment, chloride ions in sea water penetrate through the concrete and lead to enhanced depassivation. After depassivation, the corrosion of rebar progresses and rust accumulates at the interface of the rebar and concrete, which leads to the cracking of concrete because of volume expansion. In turn, the cracking considerably facilitates the penetration of CO_2, chloride ions, and water, leading to the further corrosion of the rebar. Recently, for the longer service life of concrete structures, hot-dip galvanized steel (HDG) bar has been used; however, the superiority of the HDG rebar over black rebar is not always proven. For this purpose, the differences in passivation behavior in sound concrete, the stability of the passive film in degraded concrete (*i.e.* thresholds of chloride and pH for the depassivation), and the corrosion behavior after depassivation need to be understood. In this study, we investigated the passivation behavior of both types of rebars in concrete, mortar, and the simulated concrete solutions.

Several corrosion studies of the HDG rebar have been conducted using concrete or a saturated $Ca(OH)_2$ solution that simulates the pore water in concrete. Tan *et al.*[1)] reported the passivation of HDG rebar within several hours after casting it in fresh concrete and concluded that the passivation was caused by the formation of calcium hydroxy zincate (CHZ: $Ca(Zn(OH)_3)_2{\cdot}2H_2O$). Tittarelli *et al.*[2)] investigated the role of oxygen in CHZ formation in the $Ca(OH)_2$ solution of different oxygen contents and concluded that CHZ was primarily formed by oxidation via oxygen rather than water. Note that CHZ formation on HDG rebar was stable when the pH was <13.3.[1,3,4)] Moreover, Zn corrosion has been investigated in alkaline solutions such as NaOH and KOH, and Zn passivation was confirmed in this manner.[5–8)] First, Zn dissolves as $Zn(OH)_4^{2-}$ and precipitates as $Zn(OH)_2$ or ZnO when the surface concentration of $Zn(OH)_4^{2-}$ reaches a certain value.[5,7–9)] Thomas *et al.*[7)] reported a Zn-passivated film of a two-layered structure in the NaOH solution of pH 12.0. The inner layer was compact ZnO (thickness: 10–50 nm) and the outer layer was a precipitated $ZnO/Zn(OH)_2$ mixture. These studies showed that Zn could be passivated by the formation of ZnO or $Zn(OH)_2$ film in concrete. There have been several studies of the passivation of HDG rebar in concrete or simulated $Ca(OH)_2$ solutions. The fundamental studies of Zn passivation have been performed in alkaline solutions; however, these studies were performed using HDG rebar or Zn electrodes. Note that there have been no comparative studies of the passivation and depassivation in alkaline solutions of HDG rebar (or zinc) and black rebar (or carbon steel (CS)). In this study, we electrochemically monitored the passivation behavior of both types of rebar in fresh concrete. Furthermore, we used electrochemical

* Corresponding author: E-mail: m.maeda0114@gmail.com
DOI: https://doi.org/10.2355/isijinternational.ISIJINT-2019-396

impedance spectroscopy (EIS) to monitor the passivation process of Zn and CS in fresh mortar and alkaline solutions of $Ca(OH)_2$ and NaOH at pH 12.5. To elucidate the passivation mechanisms, we performed the polarization measurements of Zn and CS in alkaline solutions.

2. Experimental Procedure

2.1. Specimens, Concrete, Mortar, and Test Solutions

We used a HDG rebar and non-coated steel (black) rebar of the same diameter (10 mm) as specimens for electrochemical impedance measurements in concrete. The thickness of the Zn coating was ~70 μm. **Figure 1**(a) shows a schematic of the concrete specimen, which was fabricated by mixing water, cement, fine aggregate and coavse aggregate at a mix ratio as shown in **Table 1**. For the impedance measurements, we embedded a couple of bars that were 30 mm apart in fresh concrete. Furthermore, the sheets of Zn (99.5%) and carbon steel (C: 0.17, Si: 0.02, Mn: 0.83, S: 0.01 wt.%) were used as specimens for electrochemical measurements in fresh mortar and alkaline aqueous solutions. These specimens were cut into 10 × 10 × 3 mm shapes and embedded in epoxy resin to act as the working electrode. For the electrochemical measurements, we used a fresh mortar and saturated $Ca(OH)_2$ solution (pH 12.5, $[Ca(OH)_2] = 1.6 \times 10^{-2}$ M) and NaOH solution (pH 12.5, $[NaOH] = 3.2 \times 10^{-2}$ M) as test solutions. Table 1 lists the contents of water, cement, and fine and coarse aggregates. They were mixed by hand at the same mixing rate for 2 min, and the cover thickness of the mortar was 10 mm. For the measurements, pH was maintained at 12.5, and the electrochemical measurements were obtained using a saturated KCl–Ag/AgCl reference electrode and a Pt wire or stainless-steel plate as the counter electrode for the solutions and mortar, respectively. Figure 1(b) shows the schematic of the electrochemical cell in the mortar. In the mortar, to properly place the reference electrode, a syringe filled with agar was inserted before curing the mortar.

Table 1. Concrete and mortar mix ratio (water–cement ratio = 0.6).

	Concrete (kg/m^3)	Mortar (kg/m^3)
Water	185	242
Ordinary Portland Cement	308	404
Fine aggregate	853	808
Coarse aggregate	917	–

2.2. Electrochemical Measurements

The electrochemical impedance of the HDG rebar in concrete was measured every hour, immediately after casting and then continued for 672 h. The impedances, Z_{10kHz} (at 10 kHz) and Z_{10mHz} (at 10 mHz), were monitored by applying AC voltage at an amplitude of 10 mV between the two electrodes. Z_{10kHz} was used for monitoring the concrete resistance, whereas Z_{10mHz}^{-1} was used as an index of the corrosion rate of the steel rebar. For the electrochemical measurements in alkaline solution and mortar, corrosion potential, E_{corr}, was immediately measured every 10 min after immersion. Electrochemical impedance spectra were obtained over the period of 20–400 h by applying AC voltage at an amplitude of 10 mV using a potentiostat (Solartron 1286) and frequency response analyzer (Solartron 1260). The frequency range was between 10 kHz and 1 mHz, and the obtained data were analyzed using Zview software (Solartron). Furthermore, anodic and cathodic polarization curves were measured at 1, 20, and 400 h using a potentiostat (Hokuto, HZ5000). The potential was scanned from E_{corr} to +2.0 V for the anodic polarization and from E_{corr} to −2.0 V for cathodic polarization at a scan rate of 1 mV/s.

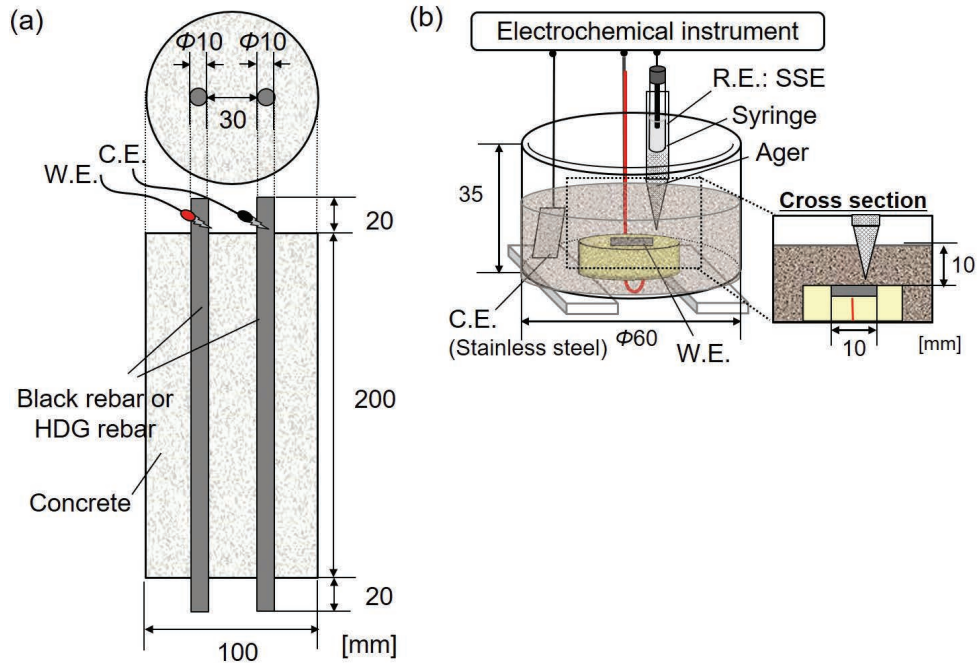

Fig. 1. Schematic of the measurement systems: (a) the top- and cross-section views of the concrete specimen, and (b) the electrochemical cell of a three-electrode cell in mortar. (Online version in color.)

2.3. Surface Observation and Analysis

We analyzed the corrosion products of the samples immersed in the solutions at various time periods. The sample surface was observed by a stereomicroscope, and the surface and cross-section were observed and analyzed using a scanning electron microscope (JEOL, JSM-6010LA) equipped with an energy dispersive X-ray spectrophotometer. For observing the cross-section, the samples were prepared using a cross section polisher (JEOL, SM-09010CP). The corrosion products were identified using X-ray diffraction (XRD) (Rigaku, MiniFlex 600) with Cu–Kα and 2θ scanned from 10° to 140°.

3. Results

3.1. Passivation of HDG and Black Rebar in Fresh Concrete

The impedance changes of Z_{10mHz} and Z_{10kHz} were measured over 672 h (28 days) (**Fig. 2**). With the rebar, it is difficult to evaluate the electrode surface area because the reinforcing bars have many ribs; therefore, the impedance per unit surface area is not shown in Fig. 2. However, because both HDG and black rebar have a similar surface area, their evaluation can be relatively compared using the impedance values. The concrete resistances (Z_{10kHz}) of both types of rebar indicated similar increases with time during the concrete curing process. A periodical fluctuation of ~10–50 Ω was observed because of daily changes in temperature as they were placed in a workspace without temperature control. The Z_{10mHz} of the black rebar increased just after immersion, and then gradually increased to reach 3 kΩ at 672 h. However, the Z_{10mHz} of the HDG rebar showed different behavior with very low values (≈100 Ω) for the first 27 h, and then a gradual increase to 7 kΩ. Noe that the HDG rebar indicated a larger Z_{10mHz} (7 kΩ) compared to the black rebar (3 kΩ) at 672 h. Finally, the HDG rebar was passivated but took longer time compared to the black rebar.

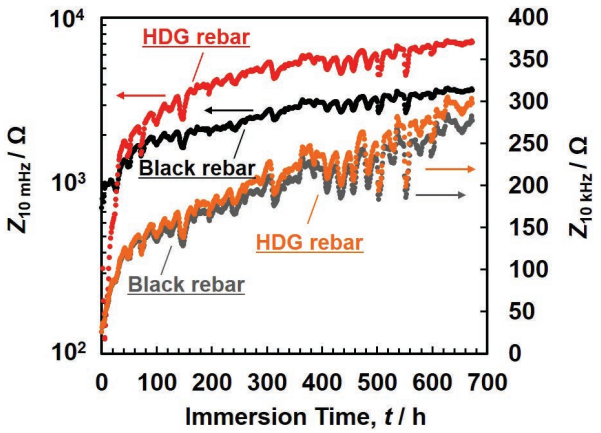

Fig. 2. Changes in the impedance at 10 mHz (Z_{10mHz}) and 10 kHz (Z_{10kHz}) of steel rebar (black rebar) and HDG rebar in concrete. (Online version in color.)

3.2. Passivation of Zn and CS in Mortar

Figures 3(a) and 3(b) show the Bode plots of Zn and CS, respectively, in mortar at 20, 100, 200, 300, and 400 h. The impedance data were fit to a one-time constant equivalent circuit (**Fig. 4**), in which R_{mor} is the mortar resistance, R_{ct} is the charge transfer resistance, and CPE is the constant phase element, which is a fitting parameter related to double layer capacitance. The symbols and lines in Fig. 3 show the experimental data and fitting results,

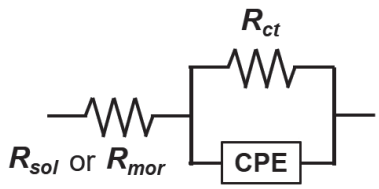

Fig. 4. Equivalent circuit used for curve-fitting of the EIS data, where R_{ct} is the charge transfer resistance, CPE is the constant phase element, R_{mor} is the mortar resistance, and R_{sol} is the solution resistance.

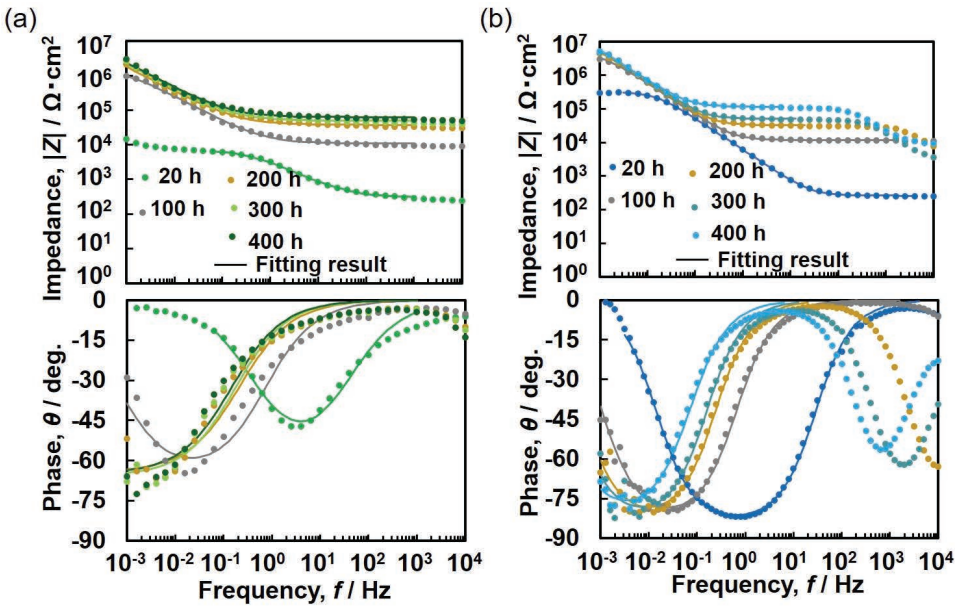

Fig. 3. Experimental results of impedance spectra on Bode diagram and fitting results of (a) Zn and (b) CS in mortar. (Online version in color.)

respectively. Other time constants (R_H and CPE_H) appeared in the high-frequency region over 10^4 Hz, possibly because of the cables and measuring device. The electrochemical impedance spectra of Zn at 20 h only showed one time constant (R_{ct}/CPE_{dl}) and fit in the frequency range of 0.1 Hz to 1 kHz. For simplicity, we performed the curve fitting of EIS data beyond 100 h using an equivalent circuit with one time constant (R_{ct}/CPE_{dl}) in the frequency range of 1 mHz to 1 kHz. All the EIS data of Zn and CS fit well within the appropriate frequency range. **Figure 5**(a) shows the changes in R_{mor} and R_{ct} in mortar obtained by curve-fitting. The R_{mor} values of Zn and CS are the order of 10^2 Ω·cm^2 at 20 h, they increased by over two orders of magnitude at 100 h, and finally reached ~10^5 Ω·cm^2 during the mortar curing process. The R_{ct} of CS in mortar was of the order of 10^6 Ω·cm^2 at 20 h, and then increased to the order of 10^7 Ω·cm^2 at 400 h. Furthermore, Zn indicated a considerably smaller R_{ct} value (<10^4 Ω·cm^2) than CS at 20 h, which increased to over 10^6 Ω·cm^2 after 100 h. Note that the R_{ct} value of Zn was comparable to that of CS. Figure 5(b) shows the change in corrosion potential, E_{corr}. After immersion, the E_{corr} of CS in mortar was around −0.4 V and then slightly shifted in the positive direction. The E_{corr} of Zn was maintained at an active potential (about −1.4 V) for the first 20 h, and then quickly shifted to a passive potential (about −0.5 V) around 20 h. From the monitoring results of R_{ct} and E_{corr}, it was found that CS was passivated just after immersion in mortar; however, it takes some time (~20 h) for Zn to be passivated. Clearly, the passivation mechanisms of CS and Zn are significantly different. The HDG rebar was active for ~30 h before passivation in concrete (Fig. 2). The amount of Zn dissolution under the active state can be roughly estimated from the obtained R_{ct} (≈ 1 kΩ·cm^2) at 1 h in mortar. Note that the corrosion rate, i_{corr}, was calculated to be 14 μA·cm^{-2} using the Stern–Geary equation:

$$i_{corr} = k / R_{ct} \quad (1)$$

where k is a proportional constant (k = 14 mV[10]). Note that the average corrosion depth for 30 h was shown to be 0.71 μm, and the obtained corrosion depth was negligibly small from the initial thickness (several tens of micrometers) of the Zn coating of the HDG rebar.

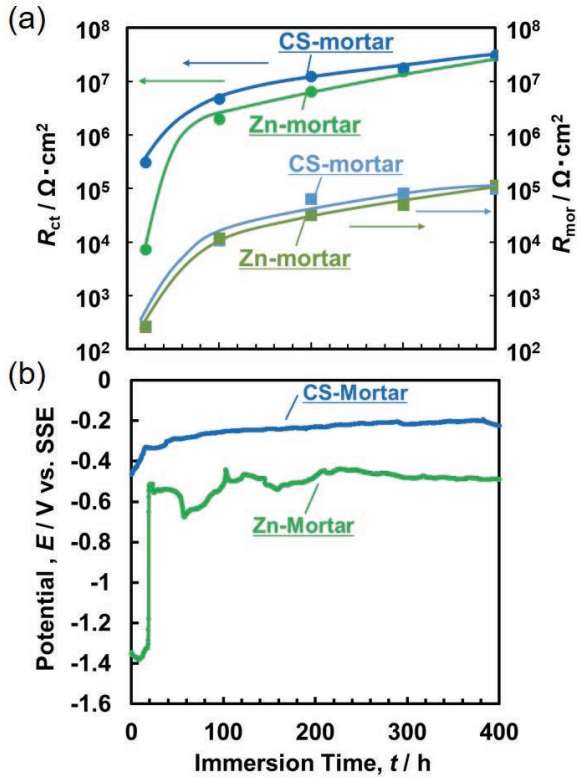

Fig. 5. Changes of (a) R_{ct} and R_{mor} and (b) E_{corr} for Zn and CS as a function of time in mortar. (Online version in color.)

3.3. Passivation of Zn and CS in $Ca(OH)_2$ Solution

Figure 6 shows the changes in the electrochemical impedance characteristics of Zn and CS with saturation time in $Ca(OH)_2$ solution (pH 12.5). Note that the symbols and lines show the experimental data and fitting results, respec-

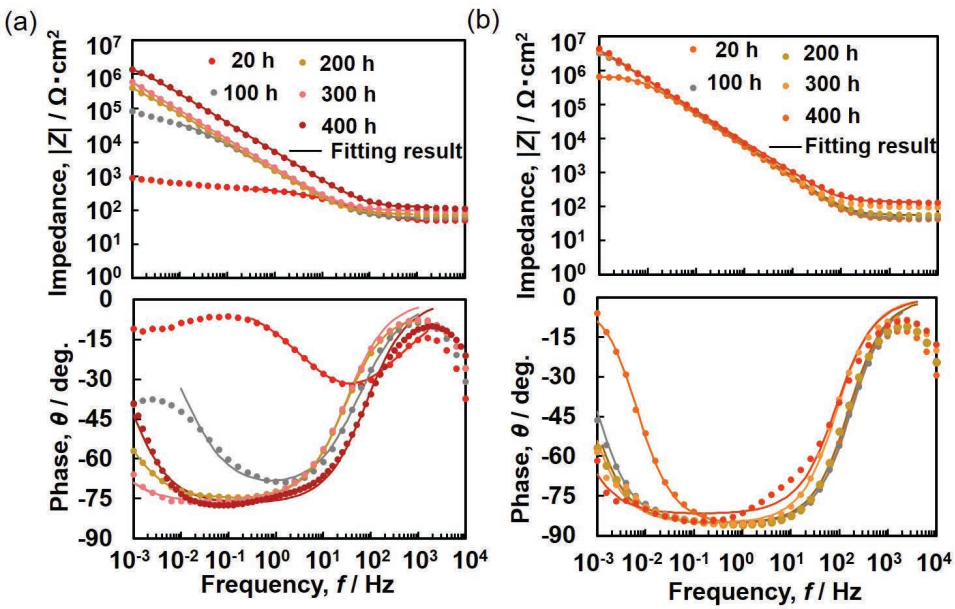

Fig. 6. Experimental results of impedance spectra on Bode diagram and fitting results of (a) Zn and (b) CS in saturated $Ca(OH)_2$ solution of pH 12.5. (Online version in color.)

tively. The impedance data were fitted similar to those in Fig. 3 using the equivalent circuit shown in Fig. 4. **Figure 7**(a) shows the changes of R_{ct} obtained by fitting in the saturated $Ca(OH)_2$ solution. The R_{ct} of Zn and CS increased with increase in immersion time; however, the increase in the rate of change of Zn was different than that of CS. The R_{ct} of CS was ~10^6 Ω·cm^2 immediately after immersion and increased to the order of 10^7 Ω·cm^2. Moreover, the R_{ct} of Zn was of the order of 10^2 Ω·cm^2 and gradually increased with time. Finally, it reached to ~10^6 Ω·cm^2, which was comparable to that of CS at 400 h. The changes in the E_{corr} of Zn and CS in the saturated $Ca(OH)_2$ solution are shown in Fig. 7(b). The E_{corr} of CS was shifted to a positive value (−0.20 V) just after immersion; however, the E_{corr} of Zn showed an active potential of about −1.3 V at the initial stage, followed by a gradual positive shift. Finally, it reached to about −0.60 V at 400 h. From the corrosion monitoring in the mortar and saturated $Ca(OH)_2$ solution, it is clear that Zn and CS will be completely passivated; however, the time to passivation for each is different. Note that Zn gets passivated after a certain time in mortar, while it gets passivated gradually in the $Ca(OH)_2$ solution because of the difference in the mass transport in mortar and aqueous solution.

3.4. Passivation of Zn in NaOH Solution

Figure 8 shows the Bode plot of Zn in NaOH solution at pH 12.5. The curve-fitting was carried out using the equivalent circuit shown in Fig. 4. **Figures 9**(a) and 9(b) show the changes in R_{ct} obtained by fitting and E_{corr}, respectively, along with those obtained in the saturated $Ca(OH)_2$ solution (pH 12.5). The R_{ct} of Zn in NaOH solution was <10^3 Ω·cm^2 and E_{corr} was around −1.3 V just after immersion, and then suddenly increased to the order of 10^4 Ω·cm^2 at 20 h, while E_{corr} quickly shifted to a positive value (about −0.55 V) because of passivation. Furthermore, the R_{ct} of Zn in

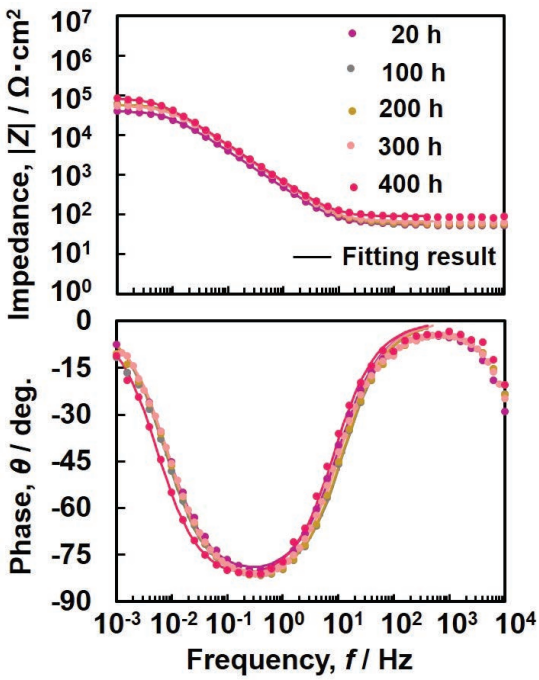

Fig. 8. Experimental results of impedance spectra on Bode diagram and fitting results of Zn in NaOH solution of pH 12.5. (Online version in color.)

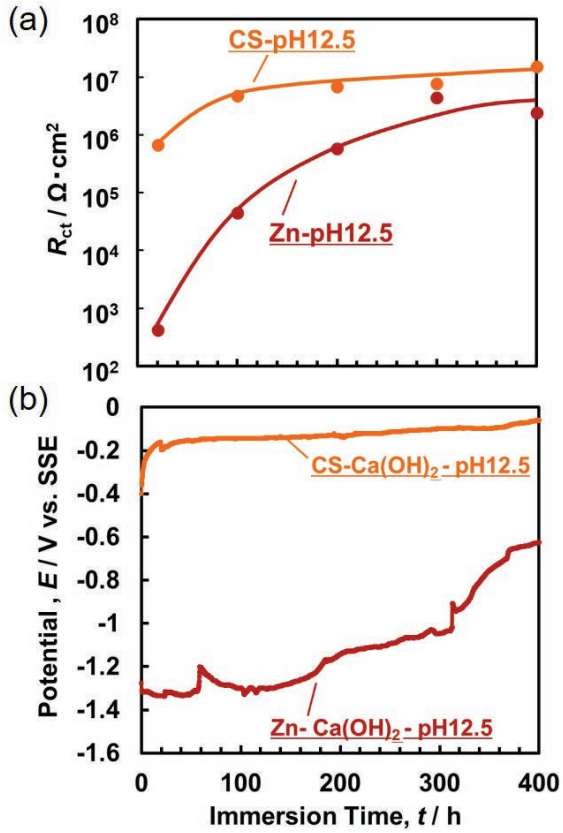

Fig. 7. Changes of (a) R_{ct} and (b) E_{corr} for Zn and CS as a function of time in saturated $Ca(OH)_2$ solution of pH 12.5. (Online version in color.)

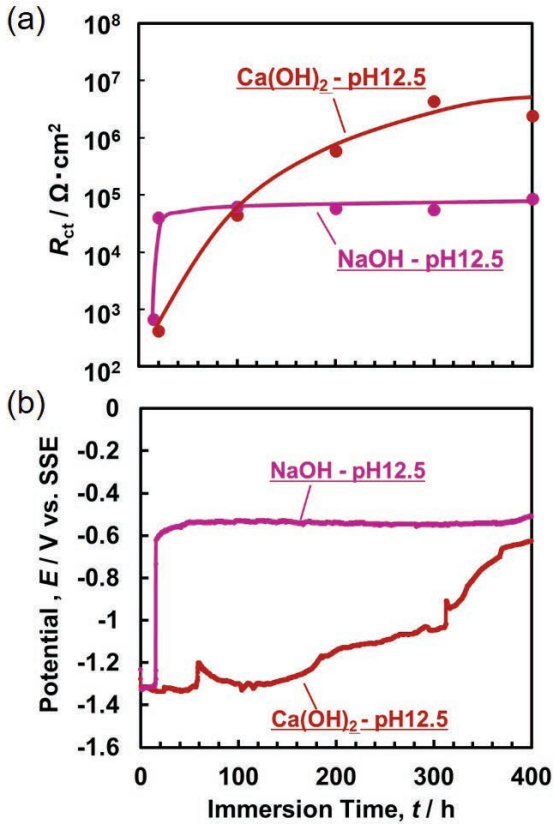

Fig. 9. Changes of (a) R_{ct} and (b) E_{corr} for Zn in $Ca(OH)_2$ and NaOH solutions at pH 12.5. (Online version in color.)

$Ca(OH)_2$ solution was less than that in NaOH solution until 100 h. Subsequently, it increased gradually to the order of 10^6 Ω·cm^2 at 400 h, while E_{corr} gradually shifted in the positive direction. Note that Zn seems to also be passivated in the NaOH solution; however, the R_{ct} in NaOH solution was almost two orders of magnitude less than that in $Ca(OH)_2$ solution. It can be expected that the passive films formed on Zn in the $Ca(OH)_2$ and NaOH solutions are considerably different. **Figure 10** shows the polarization curves of Zn in $Ca(OH)_2$ and NaOH solutions at pH 12.5 after 400 h-immersions, along with those of CS at 60 h. At the cathodic polarization, a distinct diffusion limiting current, i_d, for the oxygen reduction reaction (ORR) appeared. The i_d for Zn (0.5 μA·cm^{-2}) in $Ca(OH)_2$ solution was two orders of magnitude less than that of the passivated CS. The i_d for Zn in NaOH solution was ~20 μA·cm^{-2}, which was similar to the value for CS. It seems that the passive films formed on CS and Zn in NaOH solution have an n-type semi-conductive property; however, the passive film on Zn in $Ca(OH)_2$ solution is insulative. Note that the passive current densities of Zn on the anodic polarization in both alkaline solutions and CS in $Ca(OH)_2$ solution were similar.

3.5. Zn Corrosion Products

Figure 11 shows the surface observations of Zn at 20 and 400 h by a stereomicroscope. **Figure 12** shows the SEM images of surface and cross-section of Zn. In mortar, the formed film was compact and columnar in shape (Fig. 12(a)). Most of the surface area was already covered at 20 h, and the size of the columnar film increased with time. For the $Ca(OH)_2$ solution, similar columnar-type films were observed on the Zn surface (Fig. 11(b)). The surface was partially covered with the columnar films at 20 h (Fig. 12(b), (i): non-covered area and (ii): covered area), and the whole surface was completely covered at 100 h. From energy-dispersive X-ray spectroscopy (EDX) analysis (**Fig. 13**(a)), Zn, O, and Ca were detected across the entire film. At both Spot 1 (outer) and Spot 2 (inner), the ratio of Zn:Ca was about 2:1, and there were no differences in the elemental ratio of Zn/Ca between the inside and outside of the film. CHZ[11] was formed in the mortar and $Ca(OH)_2$ solution. In the NaOH solution, fine columnar films were formed on the Zn surface (Fig. 12(c)), and the film thickness was ~1 μm at 20 h and remained almost unchanged until 400 h. This film was determined to be ZnO or $Zn(OH)_2$ from Spot 3 in the EDX analysis (Fig. 13(b)). **Figure 14** shows the XRD patterns at different immersion times, and the show the results of up to 50° at which the film peak appears. For Zn exposed to mortar and $Ca(OH)_2$ solution, peaks assigned to CHZ, *i.e.*, 14.18°, 28.59°, 31.77°, were observed. Both ZnO and $Zn(OH)_2$ were detected in the NaOH solution.

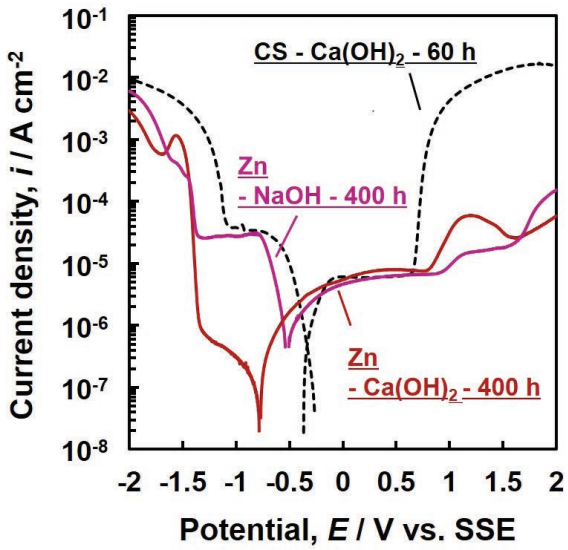

Fig. 10. Polarization curves of Zn and CS in $Ca(OH)_2$ and NaOH solutions at pH 12.5. They were measured after 400 h-immersion for Zn and after 60 h-immersion for CS. (Online version in color.)

4. Discussion

4.1. The Stability of Oxide Films in $Ca(OH)_2$ and NaOH Solutions

The stability of CHZ formed in the saturated $Ca(OH)_2$ solution was thermodynamically tested by comparing with the ZnO/$Zn(OH)_2$ formed in the NaOH solution. The equilibrium reactions are expressed using Eqs. (2), (3), and (4) between $Zn(OH)_4^{2-}$/ZnO, $Zn(OH)_4^{2-}$/$Zn(OH)_2$, and $Zn(OH)_4^{2-}$/CHZ, respectively:

$$Zn(OH)_4^{2-} \rightleftarrows ZnO + 2OH^- + H_2O \quad \text{..... (2)}$$

$$Zn(OH)_4^{2-} \rightleftarrows Zn(OH)_2 + 2OH^- \quad \text{..... (3)}$$

$$2Zn(OH)_4^{2-} + Ca^{2+} + 2H_2O \rightleftarrows Ca(Zn(OH)_3)_2 \cdot 2H_2O + 2OH^- \quad \text{.... (4)}$$

The ΔG^o of Eqs. (2), (3), and (4) are determined using the standard Gibbs free energy, ΔG_f^o, of species as follows:

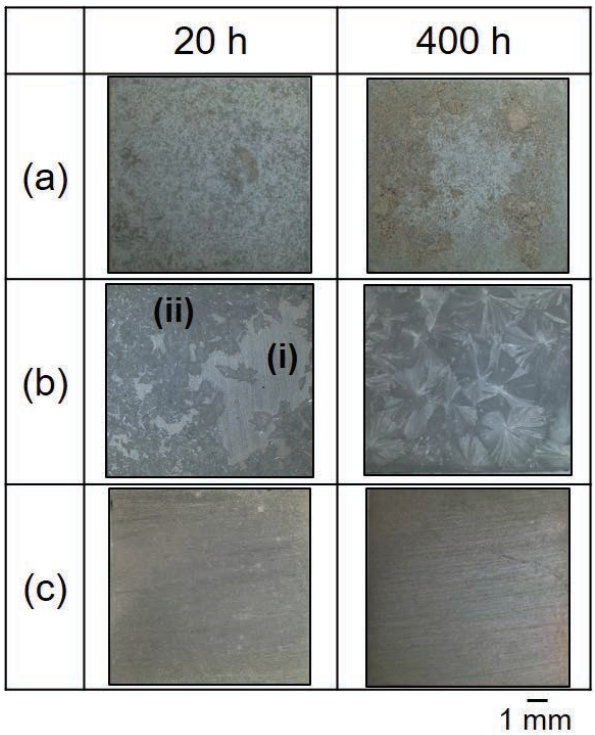

Fig. 11. Surface images of zinc exposed for 20 and 400 h to (a) mortar, (b) saturated $Ca(OH)_2$ solution (pH 12.5), and (c) NaOH solution (pH 12.5). (Online version in color.)

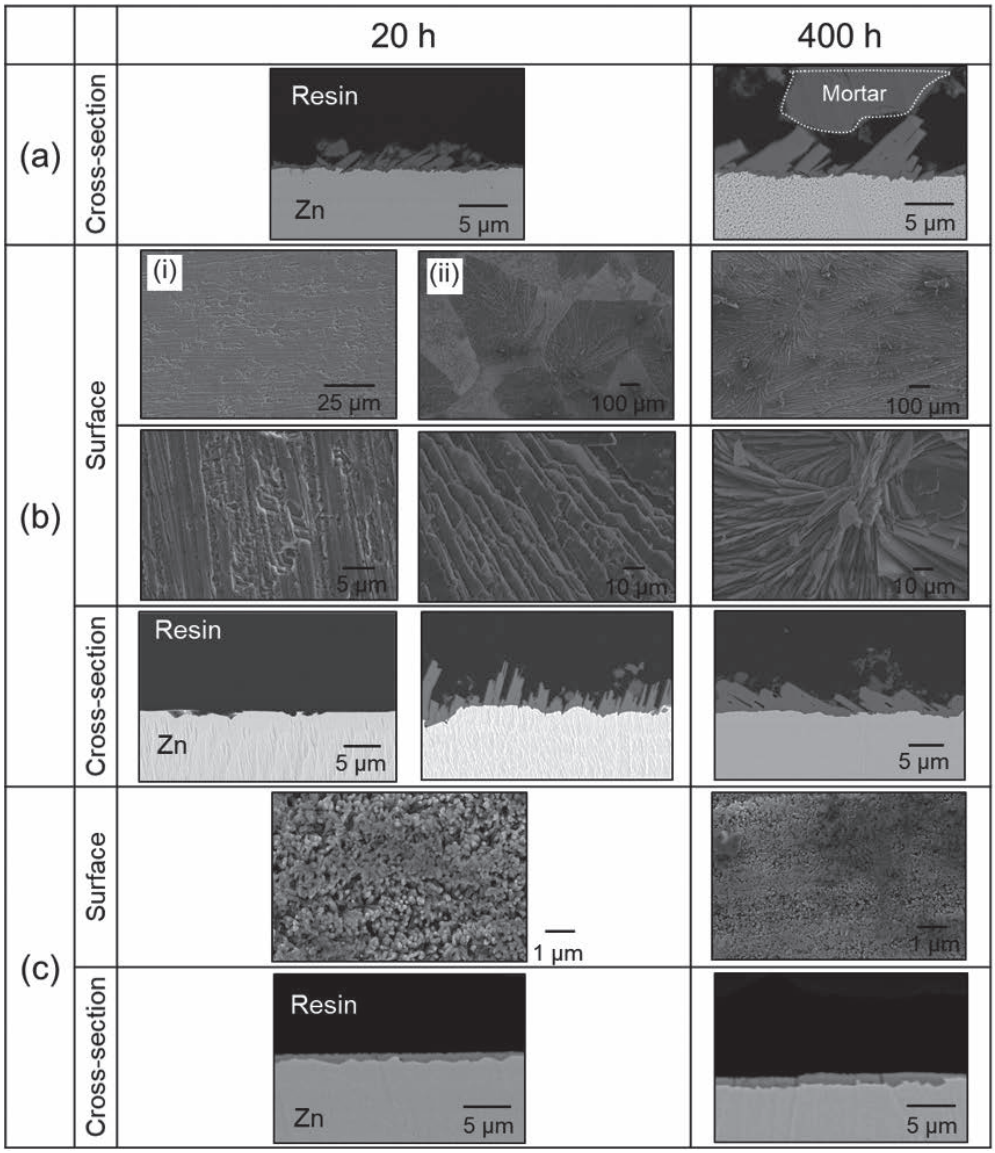

Fig. 12. Surface and cross-section SEM images of Zn exposed for 20 and 400 h to (a) mortar, (b) $Ca(OH)_2$ solution (pH 12.5), and (c) NaOH solution (pH 12.5). The bright (i) and dark (ii) surface areas in Fig. 11 correspond to (b)–(i) and (b)–(ii), respectively.

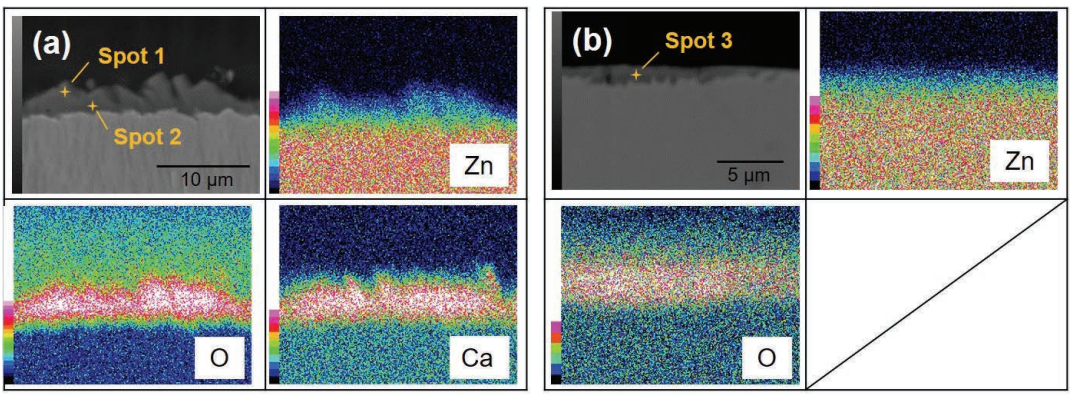

	Spot 1	Spot 2	Spot 3
Element	Atomic %		
O	30.02	40.75	21.75
Ca	3.52	7.40	—
Zn	6.82	12.68	12.31

Fig. 13. SEM images and EDX analysis of the cross-sections of films formed by exposure for 400 h to (a) $Ca(OH)_2$ solution (pH 12.5) and (b) NaOH solution (pH 12.5). (Online version in color.)

$$\Delta G^{o}_{Eq2} = \Delta G^{o}_{f.(ZnO)} + 2\Delta G^{o}_{f.(OH^-)} + \Delta G^{o}_{f.(H_2O)} - \Delta G^{o}_{f.(Zn(OH)_4^{2-})} \quad \text{..... (5)}$$

$$\Delta G^{o}_{Eq3} = \Delta G^{o}_{f.(Zn(OH)_2)} + 2\Delta G^{o}_{f.(OH^-)} - \Delta G^{o}_{f.(Zn(OH)_4^{2-})} \quad \text{... (6)}$$

$$\Delta G^{o}_{Eq4} = \Delta G^{o}_{f.(CHZ)} + 2\Delta G^{o}_{f.(OH^-)} - 2\Delta G^{o}_{f.(Zn(OH)_4^{2-})} - \Delta G^{o}_{f.(Ca^{2+})} - 2\Delta G^{o}_{f.(H_2O)} \quad \text{..... (7)}$$

By substituting $\Delta G^{o}_{f.(ZnO)}$ = −320.479 kJ·mol^{-1};[12] $\Delta G^{o}_{f.(OH^-)}$ = −157.298 kJ·mol^{-1};[12] $\Delta G^{o}_{f.(H_2O)}$ = −237.129 kJ·mol^{-1};[12] $\Delta G^{o}_{f.(Zn(OH)_4^{2-})}$ = −860.59 kJ·mol^{-1};[12] $\Delta G^{o}_{f.(Zn(OH)_2)}$ = −555.82 kJ·mol^{-1};[12] $\Delta G^{o}_{f.(CHZ)}$ = −2 501.82 kJ·mol^{-1};[15] and $\Delta G^{o}_{f.(Ca^{2+})}$ = −552.790 kJ·mol^{-1} [13] into Eqs. (5)–(7), one can obtain ΔG^{o}_{Eq4} = −11 614 kJ·mol^{-1}, ΔG^{o}_{Eq5} = −9 826 kJ·mol^{-1}, and ΔG^{o}_{Eq5} = −68 188 kJ·mol^{-1}. The solubility products, K_S, of Eqs. (2), (3), and (4) are shown in Eqs. (8), (9), and (10), respectively, using activity, a, of the involved species ($a_{(ZnO)}$ = 1, $a_{(H_2O)}$ = 1, $a_{(Zn(OH)_2)}$ = 1, and $a_{(CHZ)}$ = 1).

$$K_{S.\,ZnO} = [OH^-]^2 / [Zn(OH)_4^{2-}] \quad \text{..... (8)}$$

$$\Leftrightarrow \log[Zn(OH)_4^{2-}] = -\log K_{S.\,ZnO} - 2 \times (14 - pH)$$

$$K_{S.\,Zn(OH)2} = [OH^-]^2 / [Zn(OH)_4^{2-}] \quad \text{..... (9)}$$

$$\Leftrightarrow \log[Zn(OH)_4^{2-}] = -\log K_{S.\,Zn(OH)_2} - 2 \times (14 - pH)$$

$$K_{S.CHZ} = [OH^-]^2 / [Zn(OH)_4^{2-}]^2 [Ca^{2+}] \quad \text{..... (10)}$$

$$\Leftrightarrow \log[Zn(OH)_4^{2-}] = (-\log K_{S.\,CHZ} - 28 + 2pH + 1.80)/2$$

($[Ca^{2+}]$ = 1.58 × 10^{-2})

The solubilities, S, of ZnO, $Zn(OH)_2$, and CHZ are calculated to be $S_{ZnO} = [Zn(OH)_4^{2-}] = 10^{-5.04}$ mol/L, $S_{Zn(OH)_2} = [Zn(OH)_4^{2-}] = 10^{-4.72}$ mol/L, and $S_{CHZ} = [Zn(OH)_4^{2-}] = 10^{-6.578}$ mol/L, using the calculated ΔG^o and Eqs. (8)–(11), respectively.

$$\Delta G^o = -2.303\, RT \log Ks \quad \text{..... (11)}$$

where R is the gas constant and T is the temperature (= 298 K). From the above calculations, the solubility of CHZ is lower than that of ZnO and $Zn(OH)_2$; therefore, the stability of CHZ is thermodynamically confirmed.

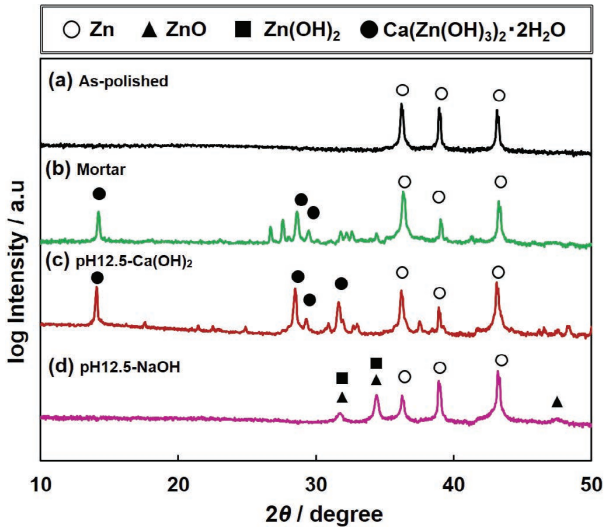

Fig. 14. XRD patterns of Zn: (a) as-polished and exposed for 400 h to (b) mortar, (c) $Ca(OH)_2$ solution (pH 12.5), and (d) NaOH solution (pH 12.5). (Online version in color.)

4.2. Passivation of Zn in Mortar and Saturated $Ca(OH)_2$ Solution

CS in saturated $Ca(OH)_2$ solution is quickly passivated just after immersion. The passive film of CS formed in simulated concrete solutions is several nanometers in thickness, where FeOOH or FeO are the inner layer, while the film mostly consists of Fe_2O_3 or Fe_3O_4 near the free surface.[14,15] In neutral solutions, Nagayama *et al.*[16] proposed a two-layer model comprising an inner magnetite layer and an outer ferric oxide layer. However, Zn will be passivated by the thicker oxide films of CHZ (several micrometers) after being kept active for a certain period of time. From the R_{ct} obtained from EIS, the protection of the passive films of Zn is almost the same as that of CS, although both passivation processes are quite different. The film formation process of

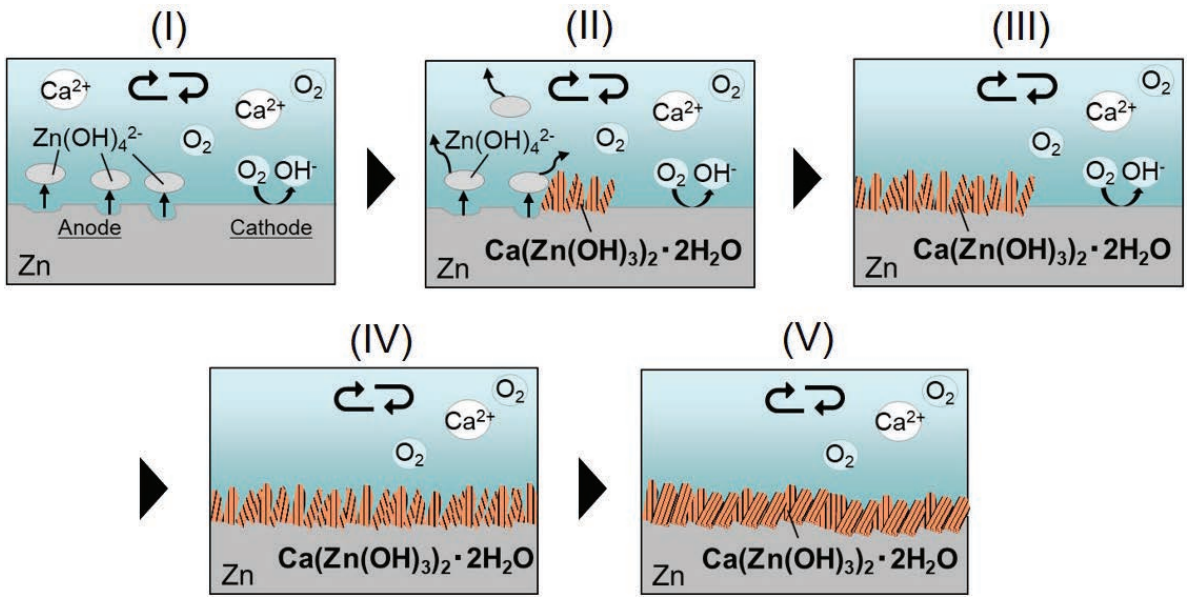

Fig. 15. Schematic of CHZ film formation in a saturated $Ca(OH)_2$ solution. (Online version in color.)

Zn in saturated $Ca(OH)_2$ solution is schematically shown in **Figs. 15**(I)–15(V). Zn dissolves as $Zn(OH)_4^{2-}$ at the anode (Fig. 15(I)) by Eq. (12):

$$Zn + 4OH^- \rightarrow Zn(OH)_4^{2-} + 2e^- \quad \text{..... (12)}$$

Then, when the surface concentration of $Zn(OH)_4^{2-}$ reaches a certain value, CHZ is deposited at the anode (Fig. 15(II)) by Eq. (13):

$$2Zn(OH)_4^{2-} + Ca^{2+} + 2H_2O \rightarrow Ca(Zn(OH)_3)_2 \cdot 2H_2O + 2OH^- \quad \text{..... (13)}$$

The coverage of the columnar-shaped CHZ deposit increases with time (III), and then most of the surface is covered with the CHZ deposit (IV). Finally, the surface passivation will be completed by a denser columnar film (V). If passivation is defined as when $R_{ct} > 10^6\ \Omega\cdot cm^2$, it will take over 200 h for Zn to be passivated by the dense CHZ film in a $Ca(OH)_2$ solution (Fig. 7). Furthermore, in fresh mortar, Zn will be passivated in a shorter time period (< 50 h) because the mass transport of the dissolved $Zn(OH)_4^{2-}$ from the surface in mortar is much slower than that in aqueous solution because there is no convection in mortar. The CHZ film on Zn will strongly suppress both anodic and cathodic reactions in a saturated $Ca(OH)_2$ solution (Fig. 10). The passive current for Zn was similar to that for CS, which indicates that the CHZ film can act as a barrier layer against the anodic dissolution, and it will be provide protection, similar to the passive film for CS. Furthermore, the ORR current of Zn was drastically suppressed by the insulative CHZ film, although it was not reduced by the semi-conductive passive film of CS (probably n-type). Thus, the CHZ film formed on the HDG rebar has comparable corrosion resistance to the passive film on black rebar in sound concrete.

5. Conclusions

The passivation behavior of HDG rebar and black rebar in fresh concrete was monitored by the continuous measuring of two frequency impedances at 10 mHz and 10 kHz. Moreover, the passivation of Zn and CS was investigated by EIS in fresh mortar, $Ca(OH)_2$, and NaOH solutions of pH 12.5. The following conclusions were drawn:

(1) In fresh concrete, the black rebar was quickly passivated, while HDG rebar was passivated after being kept active for ~30 h. The corrosion loss of Zn coating for the initial active period was estimated to be <1 μm, which is negligibly small compared with the initial coating thickness (70 μm). The corrosion rate of both types of rebar after complete passivation seems comparable.

(2) Similar to HDG rebar in fresh concrete, Zn was passivated after a certain time period in fresh mortar and saturated $Ca(OH)_2$ solution. Time to passivation in fresh mortar was considerably shorter than that for $Ca(OH)_2$ solution because the diffusion of the dissolved zincate ions may be suppressed in mortar without convection.

(3) The passivation of Zn in concrete will be caused by considerably thick CHZ films (thickness: several micrometers), which is different than iron as it is passivated by very thin oxide films (thickness: several nanometers). The concentrate of the dissolved zincate ions on the surface is very important for the passivation of Zn.

(4) The stability of CHZ in saturated $Ca(OH)_2$ solution simulating water in concrete pores was thermodynamically confirmed.

REFERENCES

1) Z. Q. Tan and C. M. Hansson: *Corros. Sci.*, **50** (2008), 2512.
2) F. Tittarelli and T. Bellezze: *Corros. Sci.*, **52** (2010), 978.
3) A. Macias and C. Andrade: *Corros. Sci.*, **30** (1990), 393.
4) A. Macias and C. Andrade: *Mater. Constr.*, **36** (1986), 19.
5) M. Mouanga and P. Berçot: *Corros. Sci.*, **52** (2010), 3993.
6) M. Cai and S. Park: *J. Electrochem. Soc.*, **143** (1996), 3895.
7) S. Thomas, I. S. Cole, M. Sridhar and N. Birbilis: *Electrochim. Acta*, **97** (2013), 192.
8) S. Szpak and C. J. Gabriel: *J. Electrochem. Soc.*, **126** (1979), 1914.
9) G. Prentice, Y. Chang and X. Shah: *J. Electrochem. Soc.*, **138** (1991), 890.
10) G. Roventi, T. Bellezze, E. Barbaresi and R. Fratesi: *Mater. Corros.*, **64** (2013), 1007.
11) C. Xavier, J. Sczancoski, L. Cavalcante, C. Paiva-Santos, J. Varela, E. Longo and M. Siu Li: *Solid State Sci.*, **11** (2009), 2173.
12) E. L. Shock, D. C. Sassani, M. Willis and D. A. Sverjensky: *Geochim. Cosmochim. Acta*, **61** (1997), 907.
13) D. A. Kulik and M. Kersten: *Environ. Sci.*, **36** (2002), 2926.
14) P. Ghods, O. Burkan Isgor, F. Bensebaa and D. Kingston: *Corros. Sci.*, **58** (2012), 159.
15) H. B. Gunay, P. Ghods, O. B. Isgor, G. J. C. Carpenter and X. Wu: *Appl. Surf. Sci.*, **274** (2013), 195.
16) M. Nagayama and M. Cohen: *J. Electrochem. Soc.*, **110** (1963), 670.